Spectroscopic measurement of temperatures in pulsed TIG welding arcs (published, see [1])

Shuiliang Ma [a,b], Hongming Gao [a], and Lin Wu [a]

[a] *State Key Laboratory of Advanced Welding Production Technology, Harbin Institute of Technology, Harbin 150001, People's Republic of China*
[b] *Plasma Research Laboratory, Australian National University, Canberra ACT 0200, Australia*

Abstract

Time resolved plasma temperatures in a pulsed tungsten inert gas (TIG) welding arc after ignition have been measured using optical emission spectroscopy. The average plasma temperatures both decrease with time in different peak and base pulse periods of the arc, and the plasma temperature decreases during the peak pulse period and increases during the base pulse period when the arc reaches the steady state. The decrease in the plasma temperature is associated with the increase in the cathode surface temperature and the decrease in the arc voltage and vise versa. The importance of the cathode surface temperature on the arc properties has been discussed.

1. Introduction

Arc plasmas characterized with high temperature and high power density are stable and can be operated with relatively low equipment cost. Due to these advantages, they are widely used in many materials processing industries, such as welding, cutting, thermal spraying and waste destruction [2,3]. In welding, tungsten-inert-gas (TIG) welding arc has been commonly used for a high quality weld since it is stable enough for control with semi-automatic and automatic welding equipment. To more precisely control the welding process, pulsed power source by controlling the arc current waveform has also been used, which is known as pulsed TIG welding. Pulsing with low frequencies less than 10 Hz is often used to control the heat input to the weld pool. Pulsing with higher frequencies is used for high-speed welding. In these applications, the product quality is strongly dependent on the arc performances. Therefore, in order to improve these applications, it is important to characterize the fundamental plasma properties, such as the electron temperature and density, the gas temperature and particle density.

Over the past years, a large amount of works have been devoted to characterizing the arc properties with different experimental techniques. Optical emission spectroscopy is a relatively simple while powerful tool which has been widely used for the diagnosis of arc plasmas. With this method, the plasma temperature and density [4–12], the cathode surface temperature [9–14], and many other arc properties have been studied, and the effects of different arc conditions, such as the operation parameters [11,13], the shielding gases [7,8], the cathode shapes and materials [9,10,14], and the anode metal vapors [6], have been extensively investigated. The measured plasma parameters are in agreement with results from other techniques, e.g. laser scattering [15]. These measurements have also shown the important role of the arc-cathode region on the plasma properties. For example, measurements by Haidar and Farmer [10] for a free-burning arc with a range of cone angles for thorated tungsten cathodes have indicated a strong dependence of the plasma temperature on the cathode surface temperature. The close connections between the cathode surface temperature and the plasma temperature and the cathode current density have also been found for a free-burning arc with pure tungsten cathode in diffuse and constrained modes [12].

Most of the previous studies on the measurement of plasma temperatures in TIG welding arcs are limited to steady state cases in which a constant current is used. However, there are many phenomena in arc discharges are time dependent, e.g., the transitions between different arc modes and the transient behavours in a pulsed TIG welding arc. It is important to measure the transient plasma properties, since they will provide more information about the processes in the plasma. The main difficulty for the time-dependent diagnosis is that, the measured optical signal is not directly related to the local plasma parameters thus a simultaneous measurement of the spatial distribution of the arc spectra with a desirable time resolution is required. With the development of technologies especially the development of high-speed charge-coupled device (CCD) detectors, the characterization of time-dependent plasma properties is no longer difficult. With a high-speed camera and narrow-band filters, we have measured the time evolution of plasma temperatures in a dc TIG welding arc after ignition, which shows interesting results that the plasma temperature decreases with time before reaching the steady state [16,17]. The decrease in the plasma temperature is considered due to the increase in the cathode surface temperature.

Numerical modelling is also important for the understanding of arc processes. Recent progress in arc plasma theory enables the cathode and anode, the electrode sheaths, and the arc column to be included self-consistently in arc models, and thus quantitative understanding of the phenomena in the arc plasma becomes possible. Based on these models, the arc properties under different conditions have been predicted, which are in good agreement with experimental measurements (see [18,19] and references therein). The development of the arc models also enables time-dependent arc properties to be investigated. Tanaka et al. [20] studied the molten pool formation and the effect the metal vapour on the TIG welding arc properties with a time-dependent model. Iwao et al. [21] calculated the temperature and the radiation power density in a TIG welding arc with several hundred hertz frequencies as a function of time, as well as the distribution of metal vapour and its effects on the arc.

Although considerable research and development in both experiments and modelling, due to the complexity of the physical processes in the arc, especially in the cathode region, there are still problems which are not fully understood, e.g., the arc voltage has not yet been possible to accurately predict [20]. For a better understanding of the physical processes occurring in these arcs and to validate the time-dependent numerical simulations, more experiments on the measurement of arc transient properties are necessary and indispensable.

In this work, we study the time-dependent properties of a pulsed TIG welding arc after ignition. Both optical and electrical techniques have been used to characterize the arc properties. The time and spatially distributed intensities of the arc were measured by using a high-speed camera with narrow-band filters. Based on the measured intensities, the plasma temperatures were obtained and the time variation trends of the cathode surface temperature were analysed. The measurements showed a strong dependence of the plasma temperature on the cathode surface temperature. The variation of the plasma temperature

Email: shlgma@126.com (Shuiliang Ma).

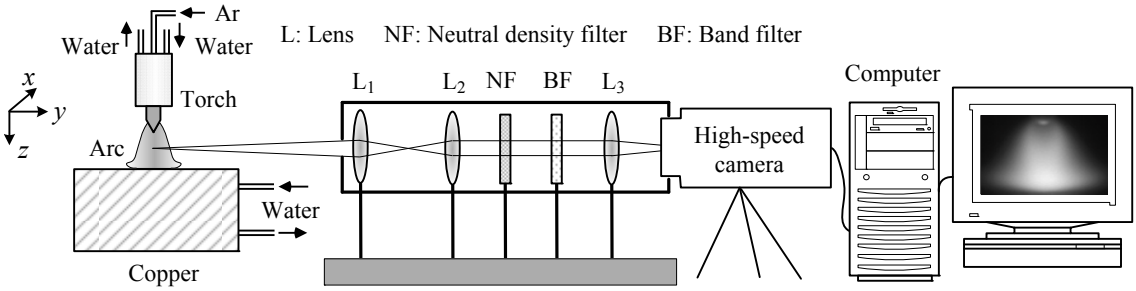

Fig. 1. Schematic diagram of the experimental set-up showing the arc generation system (left) and the filter spectrometer measurement system.

was also associated with the variation of the arc voltage. The underlying physical mechanisms behind these phenomena were discussed.

2. Experimental detail and procedures

2.1. *Arc plasma source*

Figure 1 shows the schematic diagram of the experimental system. In this experiment, the arc conditions were similar to those used in pulsed TIG welding, except that the anode was replaced by a stationary water-cooled copper plate. A welding power supply (Kemppi, Pro5000) and a TIG welding torch were used to generate the arc. After the arc had been ignited by contact ignition method, it was free burning at atmospheric pressure in argon between two water-cooled electrodes. The cathode was a thoriated tungsten rod (diameter 2.4 mm) ground to a conical tip with an included angel 60°, and the copper-plate anode was situated vertically bellow the cathode at a distance of 5 mm from the cathode tip. Argon (99.9% pure) was used as the shielding gas feeding from the cathode nozzle with a flow rate of 10 L/min. The arc parameters, such as the currents of the peak and base pulse periods, I_p and I_b, the pulse frequency, f, and the duty cycle, $k = \tau_p/(\tau_p + \tau_b)$, where τ_p is the peak pulse time and τ_b is the base pulse time, all can be adjusted to control the energy input to the welding arc. The arc current and voltage as two basic parameters of the arc were synchronously measured using a Hall-effect transducer with a sampling frequency of 10 kHz.

2.2. *Spectral measurement*

Radiations from the arc were measured using a filter spectrometer, which consists of lenses, neutral density and narrow-band filters, and a high speed camera, as shown in figure 1. The arc was observed in a direction perpendicular to the *x*-*z* plane. The origin of the coordinate system was set at the cathode tip and the positive direction of the *z*-axis pointed from the cathode to the anode. Lens L_1 was placed far away from the arc, thus the parallel-ray projection condition assumed in the Abel inversion can be approximately satisfied. Lens L_2 was used to collimate the light to ensure it perpendicularly passed through the narrow-band filter. In this way, the central wavelength of the narrow-band filter was not shifted and the interested spectral radiation can be measured accurately. After passing through the filter, the light was focused by lens L_3 at the image plane of the camera detector. The camera (Dalsa, CA-D6-0256W) was capable of capturing 8-bit grey images (260×260 pixels corresponding to the CCD sensor size of 2.6×2.6 mm^2) at a frame rate of 955 Hz. The spatial resolution in the measurement was about 0.08 mm. Due to the strong intensity from the arc, neutral density filters were placed in the front of the narrow-band filter to obtain images with strong intensity, but free from the effect of saturation.

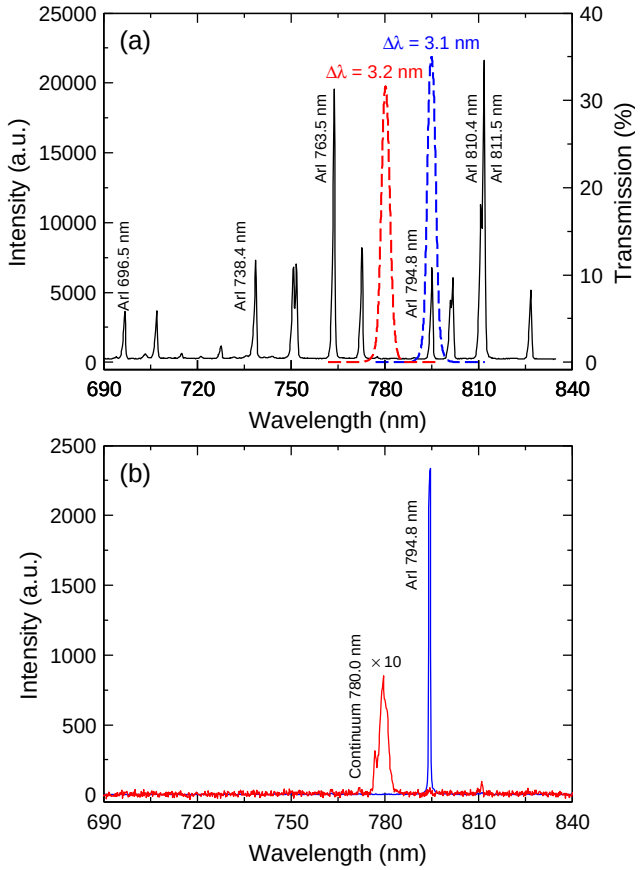

Fig. 2. (a) Emission spectrum (solid line) between 690 and 840 nm measured at $z = 1.0$ mm for a free-burning argon arc with arc current of 200 A, and transmission curves (dashed line) of two narrow-band filters with the central wavelength at 780 and 794.8 nm for the measurement of continuum and spectral line radiation, respectively. (b) Emission spectra of the arc measured with the two narrow-band filters.

The arc spectra were recorded by a grating spectrometer (details can be found in [22]) before the experiment. Figure 2(a) shows the arc spectrum in the wavelength range 690–840 nm measured in the arc cathode region at a distance of 1 mm from the cathode tip, which is mainly dominated by the Ar I spectral lines. The Ar I 794.8 nm line and the near continuum radiation at 780 nm are used to characterize the plasma properties. One reason that we choose the Ar I 794.8 nm line is that it is well separated from other spectral lines and has a strong intensity. The corresponding narrow-band filters used for the measurement of these arc radiations have a full width at half maximum (FWHM) of about 3 nm. The transmission curves for the two narrow-band filters are presented in figure 2(a) and the arc spectra that passed through the filters are shown in figure 2(b). It is seen that the spectral radiations out of the filter bandwidth are blocked by the filter, even for the continuum radiation the strong spectral lines on both sides of the filter bandwidth are almost completely blocked. Therefore, the performance of the

two filters is good and the measured plasma radiations are reliable.

2.3. *Diagnostic method*

The plasma temperature and particle density in a free-burning arc can be determined from measured spectral line and continuum radiations emitted from the arc by various methods. The methods based on, such as the relative spectral line intensity, the intensity ratio of two or more spectral lines, and the ratio of line-to-continuum radiation, have been widely used for the characterization of plasma properties [23]. In this paper, we use the Fowler-Milne method [24] to determine the plasma temperature from the radial distribution of measured relative spectral line emissions.

For an optically thin plasma under local thermodynamic equilibrium (LTE), the emission coefficient of an atomic spectral line for a transition from a level m to a lower level n can be expressed as [23]

$$\varepsilon_{\mathrm{l}} = \frac{hc}{4\pi\lambda} g_m A_{nm} \frac{n_j}{U_j} \exp\left(-\frac{E_m}{kT}\right), \tag{1}$$

where c, h, and k are, respectively, the speed of light, Planck's constant, and Boltzmann's constant, λ is the wavelength of the radiated spectral line, A_{nm} is the transition probability from level m to level n, g_m and E_m are, respectively, the statistical weight and energy of the upper level of the transition, n_j and U_j are the number density and the partition function of the species j.

The continuum radiation of plasmas containing only rare gases is composed of emissions from collisions of electrons with atoms and ions. For an argon plasma, the amount of radiation generated by the collision between electrons and atoms is less than 1% for plasma temperatures above 8000 K and thus can be neglected [25]. Ignoring the contribution of the electron-atom radiation, the continuum radiation of the free-free and free-bound emissions due to the collisions between electrons and ions is given by [25–27]

$$\varepsilon_{\mathrm{c}} = C_{\mathrm{ei}} \frac{n_{\mathrm{e}}}{\lambda^2 \sqrt{T_{\mathrm{e}}}} \sum_{i=1}^{2} n_i Z_i^2 \xi_i(\lambda, T_{\mathrm{e}}), \tag{2}$$

where $C_{\mathrm{ei}} = 1.632 \times 10^{-43}$ $\mathrm{Jm^4K^{1/2}s^{-1}sr^{-1}}$, λ is the wavelength of the continuum radiation, T_{e} and n_{e} are the electron temperature and density, n_i is the ion density, Z_i is the charge number of the ion, and ξ_i is the total Biberman factor, which is defined as

$$\xi_i(\lambda, T_{\mathrm{e}}) = \exp\left(-\frac{hc}{\lambda k T_{\mathrm{e}}}\right) \xi_i^{\mathrm{ff}}(\lambda, T_{\mathrm{e}}) + \left[1 - \exp\left(-\frac{hc}{\lambda k T_{\mathrm{e}}}\right)\right] \xi_i^{\mathrm{fb}}(\lambda, T_{\mathrm{e}}). \tag{3}$$

with ξ_i^{ff} and ξ_i^{fb} being the so-called free-free and free-bound Biberman factors.

The Fowler-Milne method, which is also known as the normal temperature method [4,5], has been widely used for the determination of plasma temperatures in high-current free-burning arcs due to advantages such as no requirement for the absolute calibration of the plasma intensity and the high measurement precision. In our experiment, continuum radiation near the wavelength of the Ar I 794.8 nm spectral line is difficult to be measured simultaneously. To reduce the effect of the continuum radiation, we have proposed a technique [22] which directly takes into account the continuum radiation in the Fowler-Milne method. Under the assumption of LTE and at an atmospheric pressure, the particle densities in the plasma as a function of temperature can be calculated based on Dalton's law, the quasineutrality condition, and Saha equations [4]. Hence, the theoretical plasma temperature dependence of the plasma emission coefficient including both the spectral line and the continuum radiation can be obtained from equations (1) and (2). According to the theoretical emission coefficient profile, the plasma temperature can be inferred from measured radial emission coefficients [4,5].

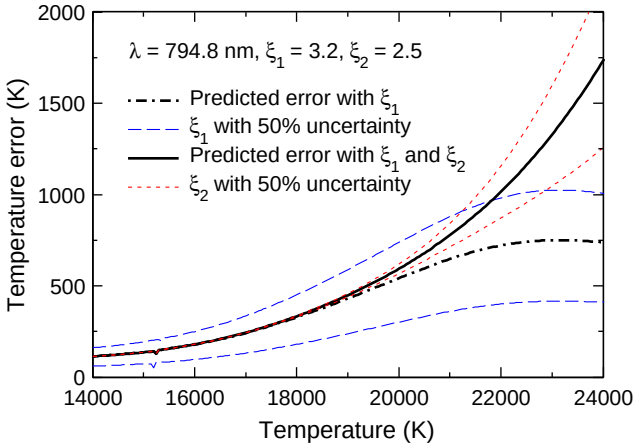

Fig. 3. Calculated temperature errors caused using the Fowler-Milne method without subtracting the continuum radiation as a function of plasma temperature. The errors due to the uncertainties in ξ_1 and ξ_2 of equation (3) are also presented. These profiles are calculated for the Ar I 794.8 nm line measured using a filter with FWHM of 3.1 nm.

Figure 3 shows the plasma temperature error profiles calculated using the Fowler-Milne method with and without subtracting the corresponding continuum radiation from the total emission coefficient at 794.8 nm for a filter with FWHM of 3.1 nm. The Biberman factors defined in equation (3) are estimated as $\xi_1 = 3.2$ and $\xi_2 = 2.5$ based on our experimental measurements [22], since the experimental values for these Biberman factors at long wavelength are in scarcity. Considering the large uncertainties in determining the values of ξ_1 and ξ_2, the temperature errors due to the uncertainties of ξ_1 and ξ_2 as a function of plasma temperature are also presented in figure 3. It is seen that without subtracting the continuum radiation, the plasma temperature determined using the Fowler-Milne method will be about 1000 K lower for a plasma temperature of 22 000 K. For lower plasma temperatures, the influence of the continuum radiation becomes smaller. The temperature error due to the continuum radiation is much lower for the Ar I 794.8 nm line compared with that for the Ar I 696.5 nm line (see [22] for details), since the Ar I 794.8 nm line has a much stronger intensity compared with that of the latter and the intensity of the continuum radiation decreases with the increase in wavelength. This is another reason why we choose this spectral line for the measurement of plasma temperatures.

Self-absorption of neutral argon spectral lines almost does not affect the plasma temperatures obtained by the Fowler-Milne method. Measurements by Bober and Tankin [28] showed that the plasma temperature determined by this method using the Ar I 763.5 nm line without considering the self-absorption of this line had a difference less than 3%. Rouffet et al [29] calculated the escape factors for several Ar I lines in an atmospheric argon plasma and showed that the escape factor of the Ar I 763.5 nm line is much smaller than that of the Ar I 794.8 nm line. Therefore, the error caused by the self-absorption of the Ar I 794.8 nm line should not be important.

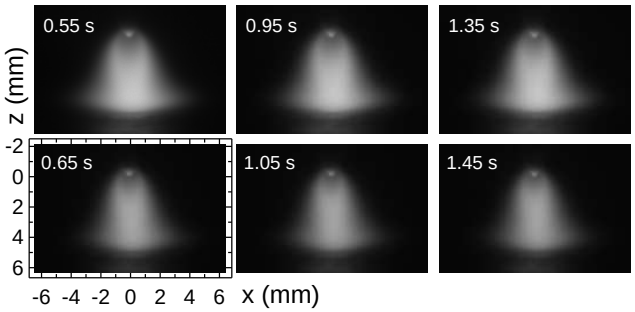

Fig. 4. A few frames of the intensity images of the Ar I 794.8 nm line acquired for a pulsed TIG welding arc ($I_p = 200$ A and $I_b = 100$ A) with several different time delays after the arc was ignited. At the top are images in three successive peak pulse periods and at the bottom are images at three successive base pulse periods.

Uncertainties in the temperature measurements due to the assumption of LTE were previously discussed in many papers (see [10] and references therein). It is generally considered that for free-burning arcs in argon, except the cathode region and the fringes of the arc, the arc central column with a plasma temperature higher than 12 800 K satisfies the LTE condition [10]. Since the LTE condition will significantly simply the diagnostics, we determine the plasma temperatures in this paper with the assumption that all regions of the arc are in LTE.

For the pulsed TIG welding arc, we only measure the plasma temperatures in the peak and base pulse periods, plasma properties during the transition from the peak to the base pulse periods and from the base to the peak pulse periods are not considered. It is shown that the relaxation times for some basic processes in an atmospheric argon plasma with a radius of 3 mm all are less than 1 ms [30]. This is in agreement with a numerical calculation which indicates that the time constant for a plasma to converge to a steady state decreases with the plasma radius and the response time constant is about 1 ms for a plasma radius of 10 mm [31]. Hence, in our experiment the TIG welding arc in the peak and base pulse periods can be treated same as that in a steady state.

3. Results

Measurements of the plasma temperature were performed for a pulsed TIG welding arc with the following parameters: peak current $I_p = 200$ A, base current $I_b = 100$ A, pulse frequency $f = 5$ Hz, and duty cycle $k = 50\%$. After being ignited by the contact ignition method, the arc current was increasing in steps to the set values in about 0.5 s.

For the determination of the plasma temperature, intensity distributions of the Ar I 794.8 nm spectral line were measured. Figure 4 shows a few typical frames of the spectral intensity images acquired with a time delay from 0.55 to 1.45 s. At the top of the figure are images measured in three successive peak pulse periods and at the bottom are images in three successive base pulse periods. The cathode tip within the arc-cathode interaction area can be clearly seen from the images due to the cathode surface radiation and the reflection of the plasma intensity by the cathode. Below the cathode tip there is a dark region in which the intensity is much lower than that in other regions. This dark region implies that the lateral spectral intensity profile is off-axis peak distributed, which is corresponding to an off-axis peak profile of the emission coefficients, thus the plasma temperature can be determined by using the Fowler-Milne method [16].

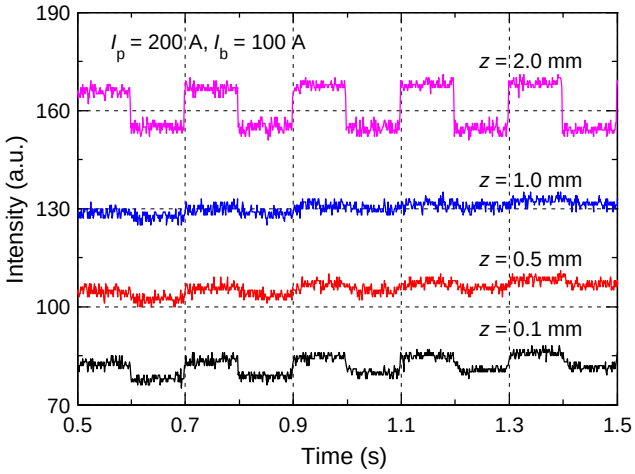

Fig. 5. Time variation of the Ar I 794.8 nm spectral line intensities at various axial positions ($z = 0.1$, 0.5, 1.0, and 2.0 mm) in the pulsed TIG welding arc.

The spectral line intensities at several axial positions of arc at distances of 0.1 to 2.0 mm from the cathode tip as a function of time are presented in figure 5. As the distance from the cathode tip increases, the difference in the intensities between the peak and base pulse periods first decreases ($z \leqslant 1.0$ mm) and then increases ($z > 1.0$ mm). Also, with the increase in time, there is a minor increase in the intensities. For the intensity profile at $z = 2.0$ mm, the increase is not apparent for the base pulse periods, while it is clear for the peak pulse periods. The variation of the intensity indicates that the arc properties change with time in different peak and base pulse periods.

To determine the plasma temperatures, side-on measured arc spectral intensity profiles with different distances from the cathode tip were symmetrised, noise filtered and Abel inverted, which yielded the radial plasma emission coefficient distributions. As a typical example, figure 6(a) shows the original and processed lateral profiles of the arc intensities measured at 0.25 mm below the cathode tip with time delays of 0.55 and 0.65 s after the pulsed TIG welding arc was ignited, which are for the peak and base pulse periods of the arc, respectively. The corresponding reconstructed radial profiles of the normalised plasma emission coefficients are presented in figure 6(b), which are off-axis peak distributed. Based on these reconstructed radial plasma emission coefficients, the plasma temperatures can then be determined using the Fowler-Milne method. The radial profiles of the plasma temperature inferred from the emission coefficients are shown in figure 6(c). The plasma temperatures near the arc center in the peak and base pulse periods are about 22 000 and 21 000 K, respectively. It should be noted that the Abel inversion has a relatively large error near the arc source center. Also, the measured lateral intensity profiles have small gradients in the arc central region. Therefore, the plasma temperature determined near the arc center has a large uncertainty. Although it is difficult to estimate the level of uncertainties, from the statistical point of view the plasma temperatures measured at different time delays should correctly reflect the changes of the arc state.

The intensity images of the Ar I 794.8 nm spectral line at different time delays were processed in a similar manner. Figure 7 shows the determined plasma temperatures as a function of time at two axial positions in the arc at distances of 0.5 and 1.5 mm from the cathode tip. The profiles are smoothed with a median filter with window size 3. It is shown that the average plasma temperatures for different peak and base pulse periods both decrease with time. For example, at the axial position

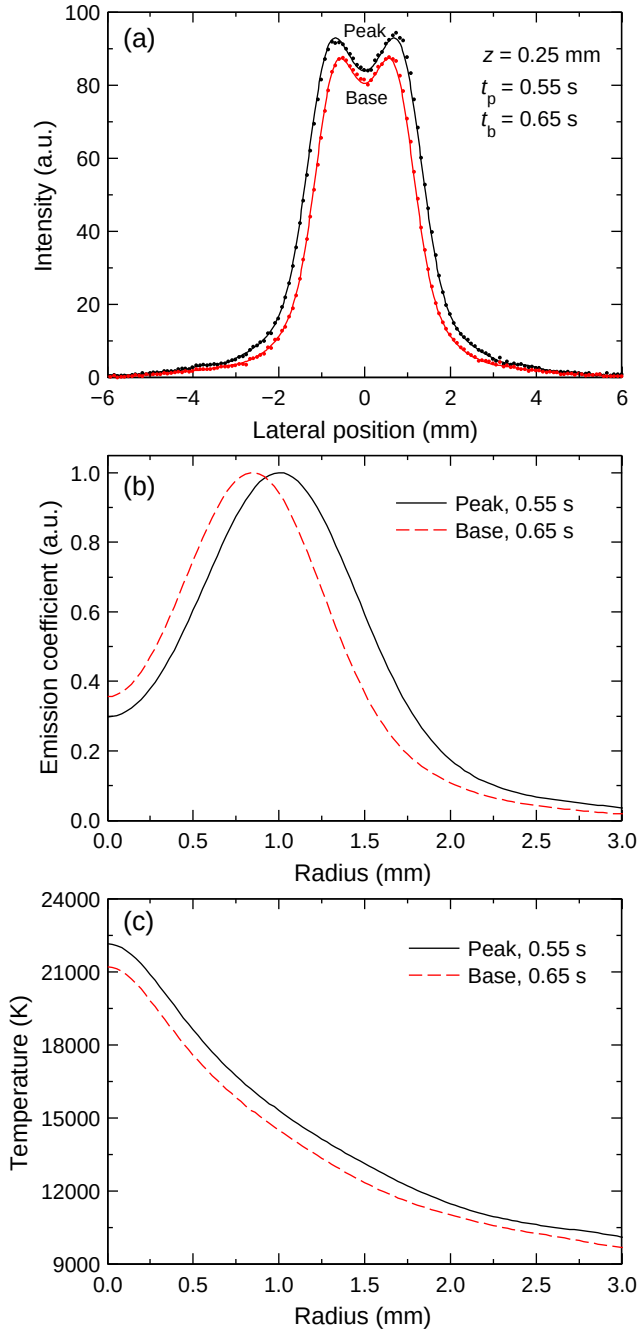

Fig. 6. (a) Lateral distributions of the arc intensities measured at $z = 0.25$ mm with time delays of 0.55 s (peak pulse period) and 0.65 s (base pulse period) for the Ar I 794.8 nm spectral line (dot) and the processed profiles (solid line). (b) The corresponding reconstructed radial profiles of the normalised emission coefficients. (c) Radial profiles of the plasma temperature inferred from the reconstructed emission coefficients.

$z = 0.5$ mm within 1 s time, the average plasma temperature for the peak pulse periods decreases from 22 800 to 21 800 K and the average plasma temperature for the base pulse periods decreases from 20 200 to 19 400 K. For each peak pulse period the plasma temperature decreases with time, whereas for the base pulse periods the plasma temperature in the first two periods first increases and then decreases with time and in the next three periods the plasma temperature always increases with time. Also, at both the starts of the peak and base pulse periods, the plasma temperature has a much more rapid decrease and increase, respectively.

Axial and radial profiles of the plasma temperature for both the peak and base pulse periods each with three time delays are compared in figure 8. These profiles are averaged in a 9 ms time interval to decrease the effects of noise and fluctuations.

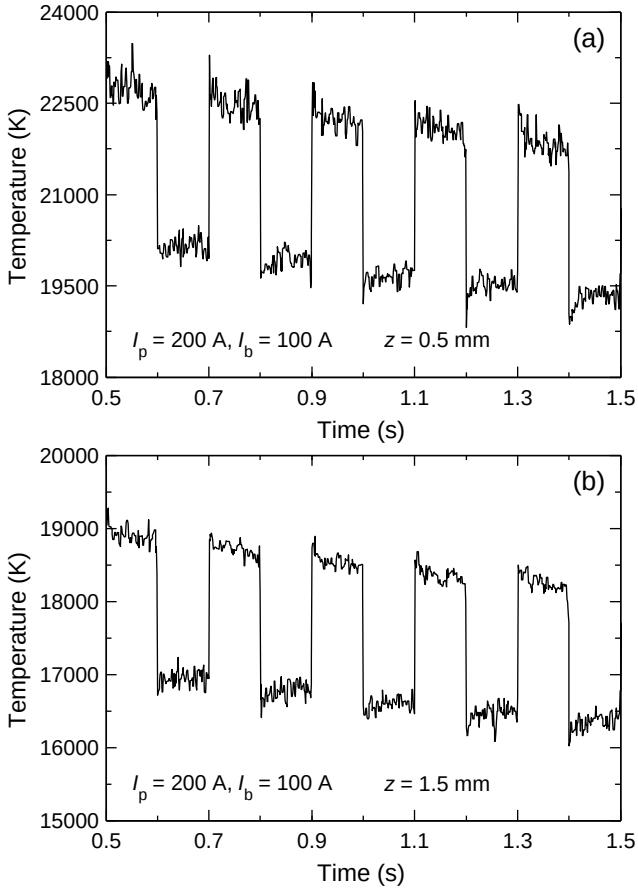

Fig. 7. Time variation of the plasma temperature at (a) $z = 0.5$ mm and (b) $z = 1.5$ mm in the pulsed TIG welding arc.

Figure 8(a) shows the axial profiles of the plasma temperature at different time delays. The plasma temperature at different axial positions for both the peak and base pulse periods decreases with time. For example, the plasma temperature at the position $z = 1.0$ mm decreases from about 20 600 to 19 900 K in the peak pulse periods ($t = 0.55$, 0.95, and 1.35 s) and decreases from about 18 600 to 17 800 K in the base pulse periods ($t = 0.65$, 1.05, and 1.45 s). The decrease in the plasma temperature at other axial positions is almost the same, about 700 K for both the peak and base pulse periods. Figure 8(b) shows the radial profiles of the plasma temperature at $z = 0.5$ mm for different pulse periods same as those in figure 8(a). The profiles show that the plasma temperature decreases with time at any radial positions in the arc. The plasma temperature has a larger decrease at the center of the arc compared with that at the edge of the arc.

Axial and radial profiles of the plasma temperature near the start and end points of both the peak ($t = 1.3$–1.4 s) and base ($t = 1.4$–1.5 s) pulse periods are compared in figure 9. Figure 9(a) shows the axial plasma temperature distributions and figure 9(b) shows the radial plasma temperature distributions. These profiles are also averaged in a 9 ms time interval. For the peak pulse period the plasma temperature at any axial and radial positions decreases with time, whereas for the base pulse period the plasma temperature at any axial and radial positions increases with time. The plasma temperature in the cathode region near the arc axis has a larger variation (about 350 K) compared with that far from the cathode region and at the edge of the arc.

In a previous experiment, we measured the time dependent plasma temperatures for a dc TIG welding arc with a current of 200 A and a 2.4 mm-diameter cathode rod, which showed the

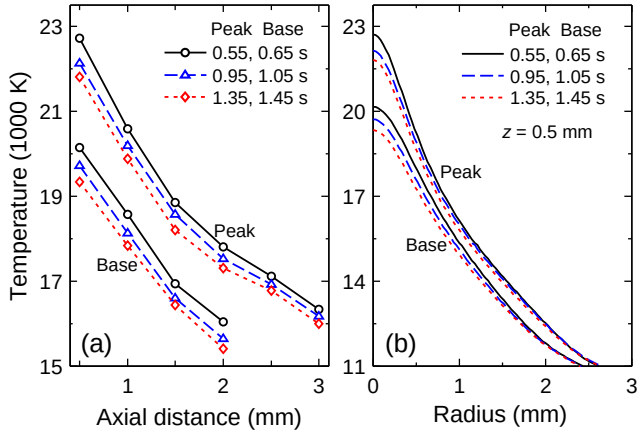

Fig. 8. Axial (a) and radial (b) profiles of the plasma temperature in three different peak ($t = 0.55$, 0.95, and 1.35 s) and base ($t = 0.65$, 1.05, and 1.45 s) pulse periods of the TIG welding arc.

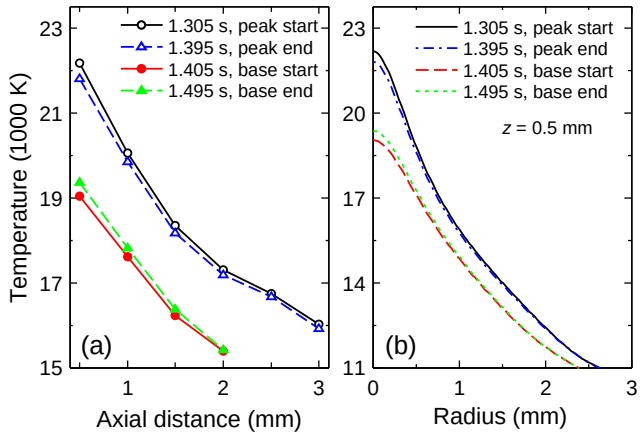

Fig. 9. Axial (a) and radial (b) profiles of the plasma temperature at the start and end points of the peak ($t = 1.3$–1.4 s) and base ($t = 1.4$–1.5 s) pulse periods of the TIG welding arc.

same decreasing trend in the plasma temperature immediately after the arc had been ignited. The decrease in the plasma temperature is most significant at the first 5–10 s. For example, at $z = 1.0$ mm near the arc axis, the plasma temperature decreased from 19 300 K to 17 800 K in about 5 s, and then decreased to 16 900 K when the arc reached the steady state. Compared with the result for the dc TIG welding arc, the plasma temperature measured for the pulsed TIG welding arc in the peak pulse periods ($z = 1.0$ mm), which also have the arc current of 200 A, is about 1300 K higher (see figure 8(a)). Considering the large uncertainties in the measurement and the different conditions for the dc and the pulsed TIG welding arcs as well as the use of the Modified Fowler-Milne method, it is believed that the measured plasma temperatures are reliable.

4. Analysis and discussion

In this section, we first analyse the factors that lead to the decrease in the plasma temperature based on the measurement of intensities from the arc cathode surface. We then discuss the relationship between the arc cathode surface temperature and the plasma temperature as well as the mechanism behind this phenomenon.

For free-burning arcs, the cathode surface temperature in the arc-cathode interaction area is difficult to measure due to the high temperature in this region, the radiation from the arc, and the reflection of the arc radiation by the cathode surface. Although optical pyrometric techniques are particularly appropriate for the measurement of high temperatures and have been widely used for the determination of cathode surface temperatures of free-burning arcs in steady state during working [9–13], it will be more difficult to measure the transient variation of the cathode surface temperature in the pulsed TIG welding arc, due to the requirement of a simultaneous measurement of the arc intensities in both spatial and wavelength dimensions with a favorable time resolution. Therefore, we only analyse the variation trend of the cathode surface temperature based on relative intensities of the radiation from the cathode surface.

Figure 10(a) shows the axial profiles of the intensity at 794.8 nm along the cathode axis in the arc peak and base pulse periods each with three time delays. It is seen that for $z > 0$ mm the intensity, which comes from the plasma, increases with time, as previously shown in figure 5. For $z < -0.7$ mm the intensity from the cathode surface increases with time for both different peak and base pulse periods. The profile of the intensity at the axis center with $z = -2.0$ mm (the insert plot) shows clearly that the cathode intensity in the peak and base pulse periods varies as a function of time. Since the intensity in this region is mainly from the radiation of the cathode surface, the variation of the intensity directly reflects the change in the cathode surface temperature. The variation of the intensity indicates that the cathode surface temperature at this position increases in all the peak pulse periods, while it increases in the first two base pulse periods and decreases in the successive three base pulse periods. For $-0.7 < z < 0$ mm the intensity decreases with time, except the region $-0.25 < z < 0$ mm in which the intensity increases with time. This zone is the arc-cathode interaction area (the axial length of the arc-cathode interaction area was about 0.9 mm for a 200 A free-burning arc [13]). The measured intensity in this area is composed of radiation from the cathode surface, the intensity from the arc, and the reflection of the arc intensity by the cathode surface. Only the radiation from the cathode surface is directly related to the cathode surface temperature. However, since the measured intensity with the central wavelength at 794.8 nm is dominated by the arc spectral line intensity and its reflection by the cathode surface, it is difficult to determine the variation of the cathode surface condition based on the measured intensity in the arc-cathode interaction area.

To more accurately determine the variation trend of the cathode surface conditions, we measured the continuum intensity distributions at 780 nm in another run with the same arc parameters as in figure 10(a). Figure 10(b) shows the axial profiles of the continuum intensity along the arc cathode axis. Although the intensity distributions in figure 10(b) are quite different, there are also some similarities: except the region $z > 0$ mm (this region belongs to the plasma), intensities in other regions have the same evolution trends compared with those in figure 10(a). For $z < -0.7$ mm, the intensity is only composed of the radiation from the cathode surface, which indicates that the cathode surface temperature is increasing with time and the variation of the cathode surface temperature in the base pulse periods changes gradually from increasing to decreasing trends (see the insert plot in figure 10(b)), same as that shown in figure 10(a). For $-0.7 < z < 0$ mm, which is the arc-cathode interaction area, the intensity increases with time except the region $-0.25 < z < 0$ mm in which the intensity decreases with time.

Spectroscopic measurements by Haidar and Farmer [9] have been shown that the radiation of the arc reflected from the cathode surface becomes negligibly low at the cathode edge. Hence, intensity in the arc-cathode interaction area measured at the edge of the cathode is only composed of radiations from

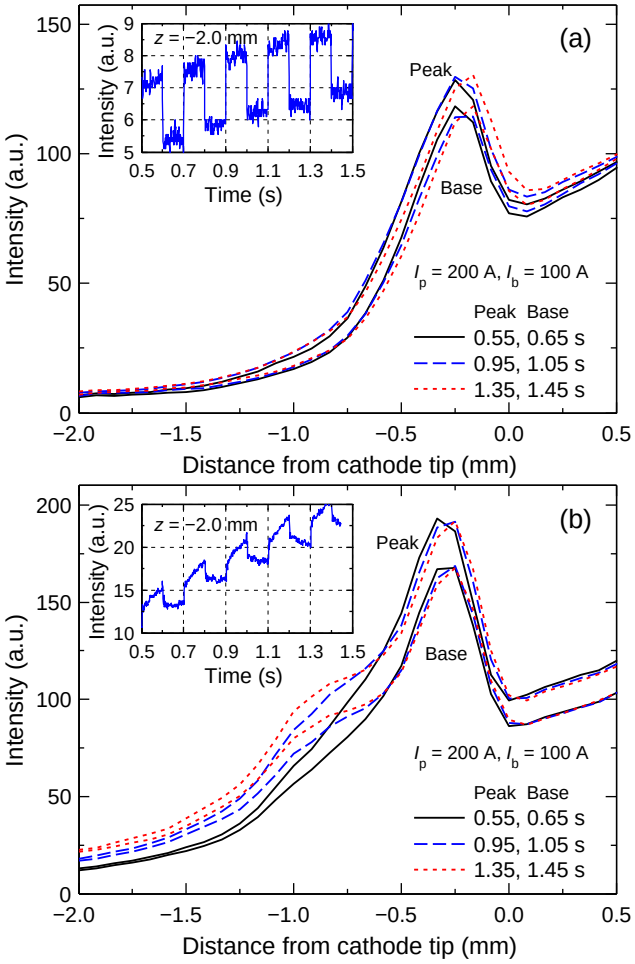

Fig. 10. Axial profiles of arc radiation along the cathode axis center in three different peak and base pulse periods for (a) the Ar I 794.8 nm line and (b) the continuum radiation at 780 nm. The inserts show the time variation of the radiations from the cathode surface at a distance of 2 mm from the cathode tip. The continuum radiation was measured in another run with the same arc conditions.

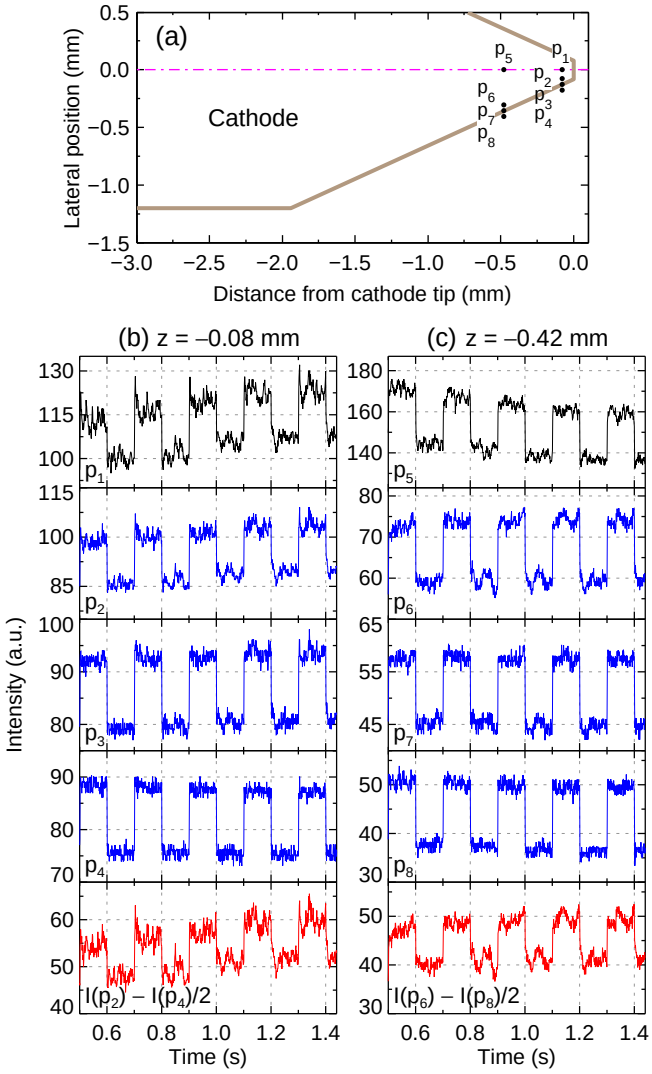

Fig. 11. (a) Schematic showing the positions of eight points (p_1 to p_8) near the cathode corresponding to eight pixels in the image. (b) and (c) Time variation of the continuum radiation at 780 nm from different positions ($z = -0.08$ and -0.42 mm, respectively) in the arc-cathode interaction area, as showing in (a). At the bottom are time variation profiles of the intensities radiated from the cathode surface at p_2 and p_6.

the cathode surface and the arc. A modified Abel inversion technique [9] can be used to remove the radiation from the arc. This technique, however, will introduce large uncertainties due to the noise amplification property of Abel inversion. In our experiment, the spatial resolution is relatively high, about 0.08 mm/pixel, so the intensities from the arc measured at two near pixels of the image are approximately the same. For the pixel corresponding to the cathode edge, the radiation from the arc therefore can be removed by subtracting half of the intensity (the reflection is from only half of the arc cross section) of the next pixel that is only viewing the radiation from the arc.

Figure 11(a) shows the positions of two sets of points at the arc image referenced to the arc cathode. These two sets of points have distances of 0.08 and 0.42 mm from the cathode tip, respectively. Points p_1 and p_5 are localised on the cathode axis center. The other points are close to the cathode edge. Points p_2 and p_6 collect the radiations from both the arc and the cathode surface, while points p_4 and p_8 only collect radiations from the arc. The intensities at these points as a function of time are shown in figures 11(b) and (c). As the points moving far away from the cathode axis in the radial direction, for $z = -0.08$ mm the variation of the intensity changes from increasing to decreasing with time, and for $z = -0.42$ mm the variation of the intensity first changes from decreasing near the axis to increasing near the cathode edge and then changes to decreasing again in the arc area. Although the intensities near the cathode axis have different variation trends, the intensities near the cathode edge have the same variation trends. Since the intensities at p_2 and p_6 (which consist of radiations from the arc and from the cathode surface; the radiation reflected by the cathode is negligible) increase with time and the intensities at p_4 and p_8 (which consist of only the radiation from the arc) decrease with time, the intensities at p_2 and p_6 radiated from the cathode surface increase with time, as shown at the bottom of figures 11(b) and (c). Therefore, it is clear that the cathode surface temperature at both p_2 and p_6 increases with time. Note that p_1 is very close to the cathode edge and thus the intensity at this point has an increasing trend and the intensity at p_5 is dominated by the radiation from the arc and that reflected by the cathode thus has a decreasing trend. These variations can also be clearly seen from figure 10(b). It is also worth noting that, compared with the radiation from the arc, the radiation from the cathode surface has relatively large fluctuations, which are possibly due to changes of the morphology of the cathode surface condition during arc working [12–14,32], thus it is difficult to determine the cathode surface temperature variation trends during different peak and base pulse periods.

The analysis of the radiation from the cathode surface together with the measured plasma temperature distributions in

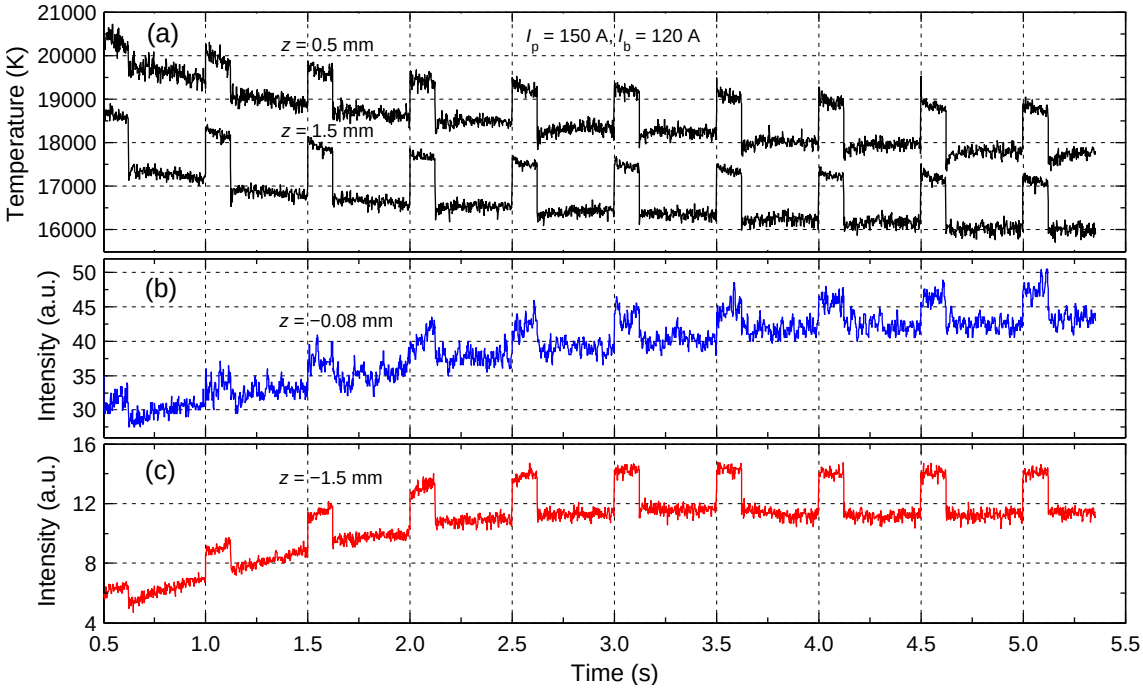

Fig. 12. Time variation of (a) plasma temperature at $z = 0.5$ and 1.5 mm, (b) arc radiation (wavelength 794.8 nm) from the cathode surface center at $z = -0.08$ mm (the intensity contributed from the arc was removed), and (c) arc radiation (wavelength 794.8 nm) from the cathode surface center at $z = -1.5$ mm for a pulse TIG welding arc with $I_p = 150$ A, $I_b = 120$ A, $f = 5$ Hz, and $k = 25\%$.

section 3 indicates the strong dependence of the plasma temperature on the cathode surface temperature. For the same arc current, a higher cathode surface temperature is always associated with a lower plasma temperature and vice versa. Since for the arc close to the steady state (a long time after arc ignition), the plasma temperature during the peak and base pulse periods decreases and increases with time, respectively, it is expected that the corresponding cathode surface temperature will increases and decreases with time, respectively.

To further test the above relationship, we measured the intensities at 794.8 nm in another run. Both the plasma temperature and the radiation from the cathode surface were obtained. Figure 12(a) shows the time variation of the plasma temperature at two axial positions at distances of 0.5 and 1.5 mm from the cathode tip. Figures 12(b) and (c) show the time variation of the radiation from the cathode surface at two axial positions $z = -0.08$ and -1.5 mm. All the profiles in figure 12 were smoothed with a median filter with window size 3. The contribution of the arc radiation at $z = -0.08$ mm was removed in a similar manner as that shown in figure 11, and thus the intensity profile also reflects the variation of the cathode surface temperature. The changes of the parameter for the pulse TIG welding arc are as follows. The peak current was decreased from 200 A to 150 A, the base current was increased from 100 A to 120 A, the pulse frequency was changed from 5 Hz to 2 Hz, and the duty cycle was lowered from 50% to 25%. In this case, compared with the previous measurement, since the heat input to the cathode during the peak and base pulse periods decreases and increases, respectively, the cathode surface temperature increases much slowly after the arc ignition and consequently it increases with time in both the peak and base pulse periods, as shown in figures 12(b) and (c). Not surprisingly, the plasma temperature decreases with time in both the peak and base periods (see figure 12(a)). After about 3.5 s when the arc has reached close to the steady state, the plasma temperature during the base pulse periods becomes increasing with time. These results are in agreement with the previous measurement and confirm the relationship between the cathode surface temperature and the plasma temperature.

The arc cathode surface temperature distribution is determined by the heat balance of a combination of processes, such as ohmic heating, thermal conduction in cathode bulk, heat transfer from the plasma to the cathode, thermionic cooling in the arc-cathode interaction area, radiation from the cathode surface, and convective cooling by shielding gas [10,32]. In our experiment, the cathode surface radiation and the gas convective cooling are not important [10,32]. After the ignition of the arc, compared with the heat loss terms the heat inputs are the dominant factors. Due to ohmic heating, the cathode bulk temperature increases. At the same time, the cathode temperature in the arc-cathode interaction area increases more rapidly, due to the heat transferred from the arc and the larger ohmic heating (because the cathode cross section is smaller in this region). Therefore, the heat conducts from the cathode tip to the cathode bulk region and the temperature over all positions of the cathode increases with time. When the cathode temperature becomes relatively high, the heat loss terms also become important and are comparable with the heat input terms. The transition of the arc from the peak pulse period to the base pulse period suddenly decreases the heat inputs, and thus the cathode temperature decreases during the base pulse period. When the arc changes from the base pulse period to the peak pulse period, the heat inputs suddenly increase, and thus the cathode temperature becomes increasing. The increase or decrease in the cathode surface temperature enlarges or reduces the region that contributes to the arc current by thermionic emission. Therefore, the current density distribution over the cathode becomes more uniform or constrained, and consequently the plasma temperature decreases or increases with time.

The close relationship between the cathode surface temperature and the plasma temperature has also been demonstrated in other experiments. Haidar and Farmer [10] have measured the plasma temperature and the cathode surface temperature distributions for a free-burning arc with a wide range of cath-

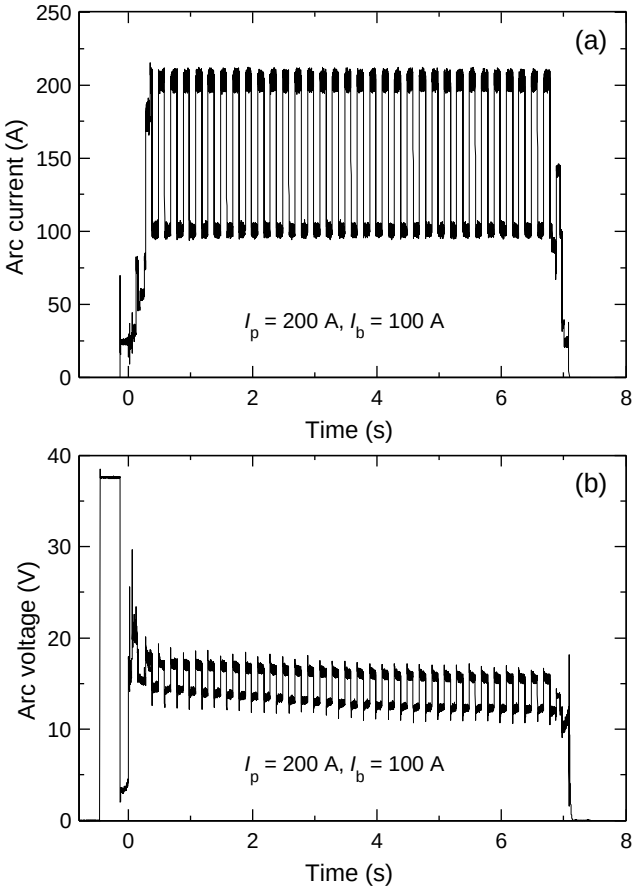

Fig. 13. Waveforms of arc current (a) and voltage (b) for the pulsed TIG welding arc after starting.

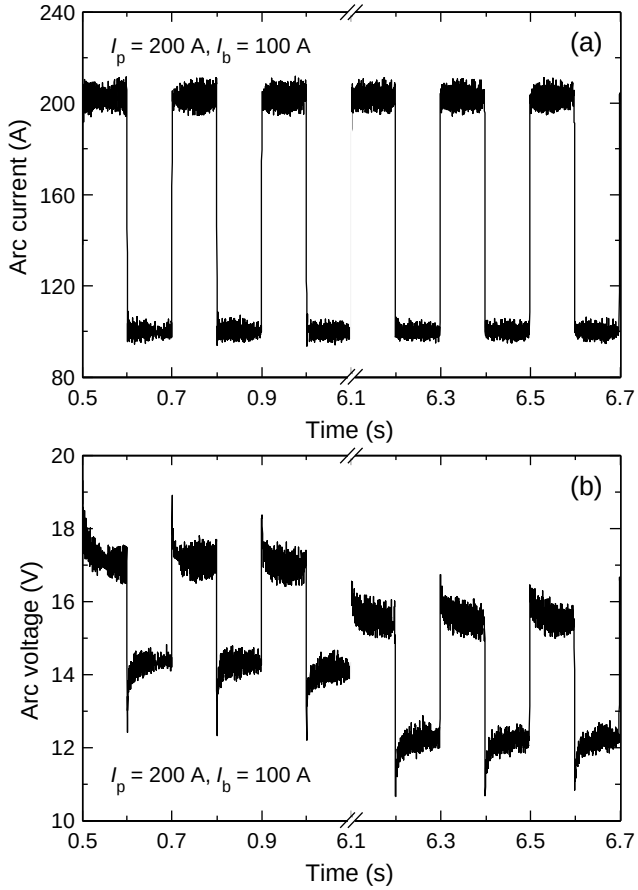

Fig. 14. Expanded timescale of the waveforms of arc current and voltage for the pulsed TIG arc after starting shown in figure 13.

ode cone angles and found the strong dependence of the plasma temperature on the cathode temperature. They have analysed the heat transfer mechanisms in the cathode region, which indicates that the largest plasma temperature for a cone angle of 60° is due to the highest current density in the arc attachment region. Mitrofanov and Shkol'nik [12] have characterized the properties of an atmospheric pressure arc with a pure tungsten cathode working in constricted and diffuse modes and shown that for the constricted mode the plasma temperature near the cathode is higher and the cathode surface temperature is lower than those for the latter. Their measurement also showed a much larger cathode current density in the constricted mode, which supports the explanation for the relationship between the plasma temperature and the cathode surface temperature.

The arc current and voltage, which are two important parameters in TIG welding, were also measured, as shown in figure 13. The arc conditions are the same as those for the determination of the plasma temperature, i.e., $I_p = 200$ A, $I_b = 200$ A, $f = 5$ Hz, and $k = 50\%$. The measurement was started before the ignition of the arc and lasted a few seconds during the working of the arc. It can be clearly seen that, immediately after the arc had been ignited by contact ignition method, there was a sudden increase in the arc voltage and the arc current was increasing in steps to the set values. The arc current was kept constant during both the peak and base pulse periods (note that the fluctuations are due to the characteristic of the welding power supply), whereas the arc voltage decreased with time from about 17 to 15.5 V for the peak pulse periods and from 14 to 12 V for the base pulse periods in about 7 s. The expanded timescales of the first and last few periods of the arc current and voltage are presented in figure 14. These enlarged profiles clearly show that in each peak and base pulse periods, the arc current is constant, while the arc voltage decreases and increases with time, respectively. The variation of the arc voltage is consistent with the variation of the measured plasma temperature. From the energy conservation point of view, the higher plasma temperature means a larger energy loss, which needs more power being input to the arc, thus the arc voltage changes with the same trend as that of the plasma temperature.

The arc voltage is composed of three parts, i.e., the potential drops in the cathode and anode regions and in the arc column. After the arc had been ignited, the plasma temperature and the temperatures over the cathode and anode surfaces gradually evolved to the steady state, thus any changes of the potential drop in one of the three parts would lead to the variation of the arc voltage. The potential drop in the arc column is almost linearly dependent on the arc length and is less likely to be the cause of the decrease in the arc voltage. The potential drop in the anode region is negative for high-current arcs (about 2 V for a 150 A argon arc) [33]. Also, it is found that the anode temperature had undetectable effects on the plasma temperature. Therefore, the variation of the arc voltage is most possibly due to the change of the cathode condition. The cathode voltage includes the potential drops in the space-charge zone ($U_s = (2.30T_e - 1.53T_c) \times 10^{-4}$ V [34], where T_e is the electron temperature and T_c is the cathode surface temperature) and in the ionization zone ($U_i = T_e/7993$ V [13,35]), and thus can be expressed as $U_c = U_s + U_i = (3.55T_e - 1.53T_c) \times 10^{-4}$ V. Based on this equation, it is seen that, when T_e changes from 25 000 to 20 000 K, U_c changes by about 1.78 V, and when T_c increases from 2000 to 3700 K, U_c decreases by about 0.26 V. These results are in agreement with the experimental measurements. Note that the voltage drop due to the change of T_c is low. Therefore, the variation of the cathode voltage is ascribed to

the changes of both T_e and T_c. This also confirms the decrease in the plasma temperature with time after the arc ignition.

5. Conclusions

Temporal variation of plasma temperatures in a pulsed TIG welding arc after ignition has been characterized by optical emission spectroscopy with a filter spectrometer. Measurements have shown that the average plasma temperature in different peak and base pulse periods of the arc decreases with time and when the arc has reached the steady state, the plasma temperature decreases and increases, respectively, during the peak and base pulse periods. Analysis of the radiation from the cathode surface indicates a strong dependence of the plasma temperature on the cathode surface temperature. The decrease in the plasma temperature is associated with the increase in the cathode surface temperature and the decrease in the arc voltage, and vise versa. The mechanism behind the phenomenon is that the increase in the cathode surface temperature enlarges the area that contribute to the arc current by thermionic emission and leads to the decrease in the current density over the cathode, consequently the plasma temperature and the arc voltage both decrease. The decrease in the cathode surface temperature has the opposite effects.

References

[1] S. Ma, H. Gao, S. Zheng, L. Wu, Spectroscopic measurement of temperatures in pulsed TIG welding arcs, J. Phys. D: Appl. Phys. 44 (40) (2011) 405202.

[2] P. Fauchais, A. Vardelle, Pending problems in thermal plasmas and actual development, Plasma Phys. Control. Fusion 42 (12B) (2000) B365–B383.

[3] U. Kogelschatz, Atmospheric-pressure plasma technology, Plasma Phys. Control. Fusion 46 (12B) (2004) B63–B75.

[4] H. N. Olsen, The electric arc as a light source for quantitative spectroscopy, J. Quant. Spectrosc. Radiat. Transfer 3 (4) (1963) 305–333.

[5] G. N. Haddad, A. J. D. Farmer, Temperature determinations in a free-burning arc. I. Experimental techniques and results in argon, J. Phys. D: Appl. Phys. 17 (6) (1984) 1189–1196.

[6] A. J. D. Farmer, G. N. Haddad, L. E. Cram, Temperature determinations in a free-burning arc. III. Measurements with molten anodes, J. Phys. D: Appl. Phys. 19 (9) (1986) 1723–1730.

[7] J. Haidar, A. J. D. Farmer, Temperature measurements for high-current free-burning arcs in nitrogen, J. Phys. D: Appl. Phys. 26 (8) (1993) 1224–1229.

[8] A. B. Murphy, Modified Fowler–Milne method for the spectroscopic measurement of temperature and composition of multielement thermal plasmas, Rev. Sci. Instrum. 65 (11) (1994) 3423–3427.

[9] J. Haidar, A. J. D. Farmer, A method for the measurement of the cathode surface temperature for a high-current free-burning arc, Rev. Sci. Instrum. 64 (2) (1993) 542–547.

[10] J. Haidar, A. J. D. Farmer, Large effect of cathode shape on plasma temperature in high-current free-burning arcs, J. Phys. D: Appl. Phys. 27 (3) (1994) 555–560.

[11] X. Zhou, J. Heberlein, Characterization of the arc cathode attachment by emission spectroscopy and comparison to theoretical predictions, Plasma Chem. Plasma Proc. 16 (1) (1996) 229s–244s.

[12] N. K. Mitrofanov, S. M. Shkol'nik, Two forms of attachment of an atmospheric-pressure direct-current arc in argon to a thermionic cathode, Tech. Phys. 52 (6) (2007) 711–720.

[13] J. A. Sillero, D. Ortega, E. Muñoz-Serrano, E. Casado, An experimental study of thoriated tungsten cathodes operating at different current intensities in an atmospheric-pressure plasma torch, J. Phys. D: Appl. Phys. 43 (18) (2010) 185204.

[14] M. Ushio, A. A. Sadek, F. Matsuda, Comparison of temperature and work function measurements obtained with different GTA electrodes, Plasma Chem. Plasma Proc. 11 (1) (1991) 81–101.

[15] A. B. Murphy, A. J. D. Farmer, J. Haidar, Laser-scattering measurement of temperature profiles of a free-burning arc, Appl. Phys. Lett. 60 (11) (1992) 1304–1306.

[16] S. Ma, H. Gao, L. Wu, S. Zheng, Time and spatially resolved spectroscopic measurement of temperatures in a free-burning arc by monochromatic imaging, Meas. Sci. Technol. 19 (10) (2008) 105602.

[17] S. Ma, H. Gao, L. Wu, Time resolved characterization of a free-burning argon arc after ignition by optical emission spectroscopy, J. Appl. Phys. 110 (2) (2011) 026102.

[18] J. J. Lowke, R. Morrow, J. Haidar, A simplified unified theory of arcs and their electrodes, J. Phys. D: Appl. Phys. 30 (14) (1997) 2033–2042.

[19] A. B. Murphy, M. Tanaka, S. Tashiro, T. Sato, J. J. Lowke, A computational investigation of the effectiveness of different shielding gas mixtures for arc welding, J. Phys. D: Appl. Phys. 42 (11) (2009) 115205.

[20] M. Tanaka, K. Yamamoto, S. Tashiro, K. Nakata, E. Yamamoto, K. Yamazaki, K. Suzuki, A. B. Murphy, J. J. Lowke, Time-dependent calculations of molten pool formation and thermal plasma with metal vapour in gas tungsten arc welding, J. Phys. D: Appl. Phys. 43 (43) (2010) 434009.

[21] T. Iwao, Y. Mori, M. Okubo, T. Sakai, S. Tashiro, M. Tanaka, M. Yumoto, Modelling of metal vapour in pulsed TIG including influence of self-absorption, J. Phys. D: Appl. Phys. 43 (43) (2010) 434010.

[22] S. Ma, H. Gao, L. Wu, Modified Fowler–Milne method for the spectroscopic determination of thermal plasma temperature without the measurement of continuum radiation, Rev. Sci. Instrum. 82 (1) (2011) 013104.

[23] H. R. Griem, Principles of Plasma Spectroscopy, Cambridge University Press, Cambridge, 1997.

[24] R. H. Fowler, E. A. Milne, The intensities of absorption lines in stellar spectra, and the temperatures and pressures in the reversing layers of stars, Mon. Not. Roy. Astron. Soc. 83 (1923) 403–424.

[25] B. Pokrzywka, S. Pellerin, K. Musiol, J. Chapelle, Experimental determination of the Ar III contribution to the continuum emission of argon at $\lambda = 468.8$ nm, J. Phys. D: Appl. Phys. 32 (14) (1999) 1665–1670.

[26] A. T. M. Wilbers, G. M. W. Kroesen, C. J. Timmermans, D. C. Schram, The continuum emission of an arc plasma, J. Quant. Spectrosc. Radiat. Transfer 45 (1) (1991) 1–10.

[27] J. J. Beulens, M. J. de Graaf, D. C. Schram, Axial temperatures and electron densities in a flowing cascaded arc: model versus experiment, Plasma Sources Sci. Technol. 2 (3) (1993) 180–189.

[28] L. Bober, R. S. Tankin, Emission and absorption measurements on a strongly self-absorbed argon atom line, J. Quant. Spectrosc. Radiat. Transfer 9 (6) (1969) 855–874.

[29] M. E. Rouffet, Y. Cressault, A. Gleizes, J. Hlina, Thermal plasma diagnostic methods based on the analysis of large spectral regions of plasma radiation, J. Phys. D: Appl. Phys. 41 (12) (2008) 125204.

[30] H. Kafrouni, Study of electron cooling, diffusion and recombination in a decaying argon arc, Physica B+C 98 (1-2) (1979) 100–112.

[31] T. Sakuta, S. Oguri, T. Takashima, M. I. Boulos, Effects of plasma diameter and operating frequency on dynamic behaviour of induction thermal plasma, Plasma Sources Sci. Technol. 2 (1) (1993) 67–71.

[32] L. E. Cram, A model of the cathode of a thermionic arc, J. Phys. D: Appl. Phys. 16 (9) (1983) 1643–1650.

[33] M. Tanaka, M. Ushio, Observations of the anode boundary layer in free-burning argon arcs, J. Phys. D: Appl. Phys. 32 (8) (1999) 906–912.

[34] M. Ushio, D. Fan, M. Tanaka, A method of estimating the space-charge voltage drop for thermionic arc cathodes, J. Phys. D: Appl. Phys. 27 (3) (1994) 561–566.

[35] W. Neumann, The Mechanism of the Thermoemitting Arc Cathode, Akademie, Berlin, 1980.